0254-6124/2022/42(5)-0884-07 *Chin. J. Space Sci.* 空间科学学报

LU Li, YU Qinglong, ZHOU Ping, JIA Shuai, CHANG Yuan. Simulation of ENA Imaging Measurements on a Geosynchronous Orbit. *Chinese Journal of Space Science*, 2022, **42**(5): 884–890. DOI:10.11728/cjss2022.05.210414051

Simulation of ENA Imaging Measurements on a Geosynchronous Orbit*

LU Li[1,2,3] YU Qinglong[1,2,3] ZHOU Ping[1,2,3]

JIA Shuai[1,2,3] CHANG Yuan[1,2,3,4]

1(*Laboratory of Space Environment Exploration*, *National Space Science Center*, *Chinese Academy of Sciences*, *Beijing* 100190)

2(*Beijing Key Laboratory of Space Environment Exploration*, *Beijing* 100190)

3(*Key Laboratory of Science and Technology on Space Environment Situational Awareness*, *Chinese Academy of Science*, *Beijing* 100049)

4(*Shanghai Institute of Satellite Engineering*, *Shanghai* 200240)

Abstract Geosynchronous orbit is located in the ring current region, where the energetic particle emission environment challenges the ion deflection design limit of the Energetic Neutral Atom (ENA) imager. Therefore, there is no measurement record of ENA imaging in this area before. On the basis of possessing the patent of high-energy ion deflection technology, ENA imaging under different *Kp* index in geosynchronous orbit is simulated. The simulation images show the characteristics of low-altitude ENA emission source and the rough sketch of magnetosphere. Due to the north-south conjugation observation of geosynchronous orbit, the simulated ENA images at different positions all have north-south symmetry. Aiming at the unsolved problems, such as the input source of ring current energetic ions during geomagnetic activities and its evolution process, we analyzed the possible results of ENA imaging combined with *in-situ* particle measurements in the same satellite, as well as the subversion effect of any north-south asymmetry of ENA map on the inversion model.

Key words Energetic Neutral Atom (ENA), Magnetosphere, Ring current, ENA imaging

Classified index P353

0 Introduction

The energy of geomagnetic activity usually comes from the input of kinetic energy of solar wind particles. However, the specific time, path and mechanism of its input have always been a puzzle in the field of magnetosphere physics. ENA imaging measurement and inversion is an important technique to reveal the particle energy transport process. Lu *et al*.[1,2] used the inversion of ENA imaging data with a high spatial and temporal resolution of NUADU/TC-2[3,4] to give preliminary results on the time series and development process of geomagnetic substorms, and proposed directions for further research. Through simulation, we can make the exploration technology more reasonable and effective to serve the above specific scientific objectives.

Previous magnetospheric ENA imaging exploration satellites mostly adopt large elliptical orbits with

* Supported by National Key R&D Program of China (2020YFE0202100), National Mission/Other National Mission: Research on Key Technologies of the Outer Heliospheric Space Exploration System (Y91 Z100102) and National Mission/National Major Science and Technology Project: CE-7 Relay Satellite Display Neutral Atom Imager (E16504 B31 S)

Received April 14, 2021. Revised January 5, 2022

E-mail: luli@nssc.ac.cn

large inclination[4–6], with apogee over tens of thousands km, and ENA emission signals from the north and south polar regions cannot be observed at the same time. The simulation and inversion models are all based on the assumption of the north-south conjugate change of the reciprocating bounce of energetic ions along magnetic lines[7–13]. The ENA imaging measurement and inversion only focus on the radial and azimuth changes of the Energetic ion distribution in the ring current region. However, the north-south conjugation properties of ENA imaging observations should also be questioned. At least, the north-south conjugate characteristics of the auroral arc in the polar cap region associated with the precipitation particles are not very clear. Xing *et al.*[14] found that the polar cap arc's motion in dawn-dusk direction shows a clear dependence on the interplanetary magnetic field B_y component and presents a clear asymmetry between Southern and Northern Hemispheres. The ENA emission signals from the north and south poles can be telemetered simultaneously on the geosynchronous orbit satellite, which is an ideal platform for detecting and tracking the source and characteristics of precipitation particles.

The geosynchronous orbit is located in the ring current region, where the energetic particle emission environment challenges the ion deflection design limit of the ENA imager. As a result, there is currently no ENA imaging exploration program in this orbit. On the basis of the design patent of the charged particle deflection device[15], we simulated the ENA imaging measurement of ENA imager under different geomagnetic activities (*Kp* index) on the geostationary orbit satellite. The causal sequence of ion transport during geomagnetic activity is analyzed by means of ENA imaging telemetry and in situ measurements of energetic particles sampling in the same local time zone on board of the same geostationary satellite.

1 ENA Imaging Simulation during Magnetic Storm

1.1 Simulated Orbit

Geosynchronous orbit altitude r = 35786 km, inclination 0° in the equatorial plane, as shown in Fig.1. Four ENA imaging simulation locations: noon, dusk, midnight and dawn are marked in Fig.1.

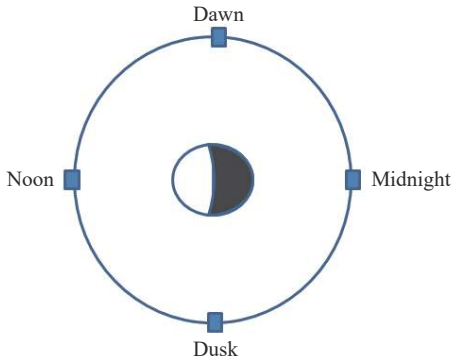


Fig. 1 Geosynchronous orbit and ENA imaging simulation positions

1.2 Simulation Equations

The counts recorded in each pixel of an ENA image, $C(\delta, \varepsilon)$ with elevation δ and azimuth ε, is represented in the simulation equation,

$$C(\delta,\varepsilon) = \int \Delta E \Delta T \Delta \Omega j_{\text{ion}}(L,\varphi,\theta,E,\alpha) A(\delta,\varepsilon)\sigma(E)n(r,\varphi,\theta)\,\mathrm{d}V. \quad (1)$$

Here ΔE is the energy range within; ΔT is the integral time for the pixel; $\Delta\Omega$ is the solid angle of the volume element pointing to the δ, ε pixel; j_{ion} is Ion differential flux at the Integral volume element; $A(\delta,\varepsilon)$ is the response function of a detector[13]; $\sigma(E)$ is the charge exchange cross sections[16]; $n(r, \varphi, \theta)$ is the exospheric neutral atomic density, where r is geocentric distance, φ is longitude, and θ is latitude; $\mathrm{d}V$ is the volume element integral along the line of sight of the detector.

The ion flux in the ring current region may be expressed in the form of[12]

$$j_{\text{ion}}(L,\varphi,\theta,E,\alpha) = e\, j_{\max 0} h(\varphi) \frac{E}{E_0}\left\{1+\left(\frac{E(L/L_0)^3}{\kappa E_0}\right)\left[\sin\alpha_{\text{eq}} + (1-\sin\alpha_{\text{eq}})(L_0/L)^{0.45}\right]^2\right\}^{-\kappa-1}. \quad (2)$$

Here,

$$e = (1+1/\kappa)^{\kappa+1} \approx 2.962(\kappa = 5.5),$$

φ is azimuth,

$$h(\varphi) = \exp\{-\xi[1-\cos(\varphi-\varphi_s)]\},$$

(Here, φ_s =180°, ξ =0.75 for azimuth asymmetry of ring

current ion flux), θ is the magnetic latitude, L is the magnetic shell index, φ is the magnetic longitude, E is the proton's energy, E_0 (7 keV) is the typical ion-energy of the maximum ion-flux, and L_0=7.3 is the outer boundary of the ion injection region of the Ring Current (RC).

In Eq. (2), the ion flux changes *vs.* magnetic shell index L is related to the magnetic activity index *Kp*. In definition of L_b=(122–10*Kp*)/(24–L_0), then:

$$L=\begin{cases} L+2(L_b-L), & L<L_b; \\ L, & L\geqslant L_b. \end{cases} \tag{3}$$

The pitch angle (α) of the particles within the volume element is expressed in terms of θ (magnetic latitude) and α_{eq} (equatorial pitch angle) such that

$$\sin\alpha=\frac{(1+3\sin^2\theta)^{1/4}}{\cos^3\theta}\sin\alpha_{eq}. \tag{4}$$

The ENA imager has a minimum energy channel of more than 10 keV, so it cannot directly record the neutral atom evaporated from the exosphere. The ENA map recorded by the ENA imager is the energetic neutral atom produced after the charge exchange of neutral atom evaporated from the exosphere and energetic ions precipitated from the ring current region.

The neutral hydrogen densities provided by Chamberlain's model adjusted by Rairden *et al.*[17] are too low to be applicable in the ring current region. If conservation of the radial flux of neutral atoms during a major geomagnetic storm is assumed, we may, however, add an additional term to the Chamberlain model so that the density can be represented by

$$n(r,\theta,\varphi)=n_0\left\{\exp\left[17.5\,\mathrm{e}^{-1.5r}-\frac{r}{1.46(1-0.3\sin\theta\cos\varphi)}\right]+\left(\frac{a_0}{r}\right)^2\right\}, \tag{5}$$

where r is the geocentric distance in R_e, a_0=1.78 R_e represents the height of the exosphere, and n_0=1600 cm^{-3} is the neutral density constant. This model is better fitted for the yearly average hydrogen density in solar maximum conditions in the ring current region measured by Tinsley *et al.*[18], which should also be suitable in a major storm period.

1.3 Simulation Results

Assuming that *Kp* index is 3, 5 and 7 respectively, the hydrogen ion flux distribution with an energy range of 10～30 keV in the equatorial ring current region is shown in Fig.2. The local time, *Kp* index, satellite orbit and ENA imaging simulation position are labeled in a certain place of each plane in Fig.2. With the increase of *Kp* index, the ion flux increases, and the maximum ion flux region moves earthward. Maximum fluxes and locations of hydrogen ion fluxes under different *Kp* indexes are given in Table 1.

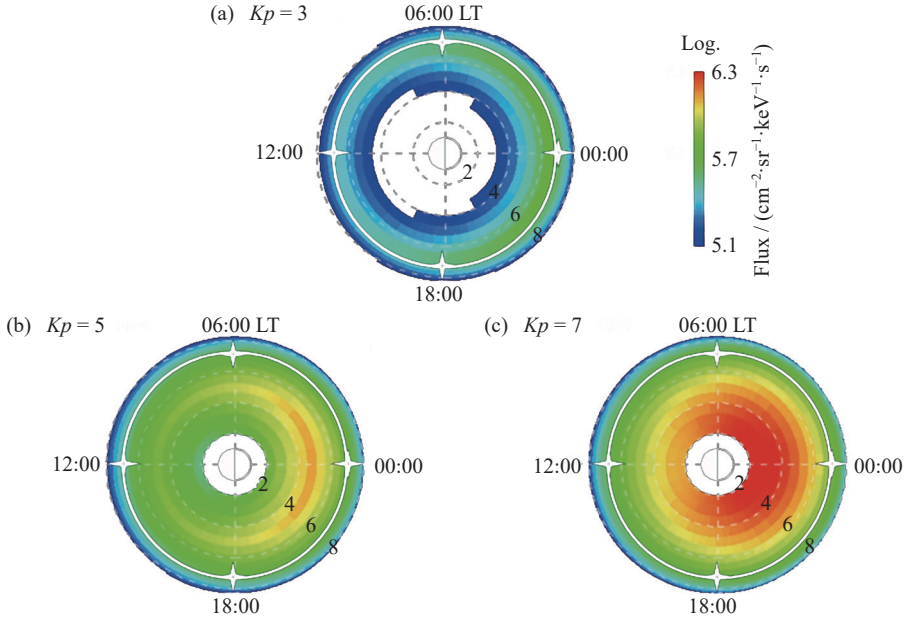


Fig. 2 Equatorial ion flux distribution with geomagnetic active index *Kp* of 3, 5 and 7, respectively

Table 1 Maximum hydrogen ion fluxes

Kp index	3	5	7
Maximum ion flux/ ($cm^{-2}\cdot sr^{-1}\cdot keV^{-1}\cdot s^{-1}$)	5.07×10^5	1.31×10^6	2.3×10^6
Location of L/R_e	6.4	4.6	3.2

For the triaxial stabilized satellite, a space Angle of 6°×6° is set for each detector unit in the 4π Field of View (FOV) of the simulation. According to the simulation model developed by Lu *et al.*[13], simulated ENA images with 1 min integration at noon, midnight, dawn and dusk at different *Kp* indexes were obtained, Fig.3. Under different geomagnetic active conditions, the maximum ENA counts of simulated images corresponding to the four local time are given in Table 2.

The effective simulated ENA count is basically distributed in 2π FOV earthward. In Fig. 3, the center of the polar coordinate system (–90°) is facing the Earth. In the FOV range of –90°～–84°, there is basically no effective simulated ENA count. The pixel distribution of the maximum ENA count tends to coincide with the magnetic field line projected at high latitudes. Especially in the case of night, line-of-sight at –90° traverses the ion flux maximum in the ring current region (see Local Time 00:00 in Fig.2), but there is still no effective ENA simulation count in the range of –90°～–84°(the 2nd row of Fig.3). This indicates that during geomagnetic activity, the exploration characteristics of the magnetosphere are usually low-altitude ENA emission sources at high latitudes[19, 20]. The region covered by the lower limit color block in those simulated ENA images vividly outlines the contour of the magnetosphere. Where, the first and second rows of Fig.3 are the magnetosphere profile at the section dawn-and-dusk, and the third and fourth rows are the magnetosphere profile at the meridian plane.

From left to right in Fig.3, as *Kp* index increases, the simulated ENA count increases and the spatial distribution range of ENA emission increases also. The simulated ENA image (Row 3 and 4 in Fig.3) observed from both sides of dawn and dusk shows the distribution characteristics of simulated ENA count along the projected magnetic field line due to the day-night asymmetry of the distribution of ring current energetic ion fluxes. The increase in the simulated ENA count in polar caps of both south and north (see the 2nd row of Fig.3) is the projection of ENA emission enhancement on the closed magnetic field line of the magnetotail in the polar region.

2 Discussion

The ion flux distribution presented by the simulation model[13] is symmetric in the morning and evening and in the north-south direction, except for the day-night asymmetry. The ENA simulation results (Fig.3) also demonstrate the above symmetry.

The exploration results show that the distribution of the equatorial ion flux is not uniform in the radial or in the azimuth[21, 22]. With the enhancement of geomagnetic activity, the distribution of ion flux in the ring current area will appear to move earthward, and it is often accompanied by east/west drift in different phases of the substorm[1, 2, 23].

Whether the distribution of ion flux has the asymmetry of north and south is a problem that has not been involved before. Because the previous ENA imaging exploration satellite has a large inclination, it cannot record ENA emission signals at the north and south poles at the same time, and it naturally does not pay attention to the asymmetry of ENA images in the south and north. Geosynchronous orbit observation, satellite record global ENA imaging at low latitudes can naturally pay attention to the symmetry between north and south of ENA emission signals.

If the north-south asymmetry of ENA emission signal appears in the actual observation, it will be subversive to the previous ENA inversion model. In previous inversion models, we always assumed that the ring current energetic ions producing ENA emission bounced back and forth between the north and south poles along the closed magnetic field line, and its corresponding ENA emission source should be symmetrical between north and south. Therefore, the contingency of the latitude variation of ion fluxes is excluded from the inversion calculation and replaced by a theoretical model[11,12].

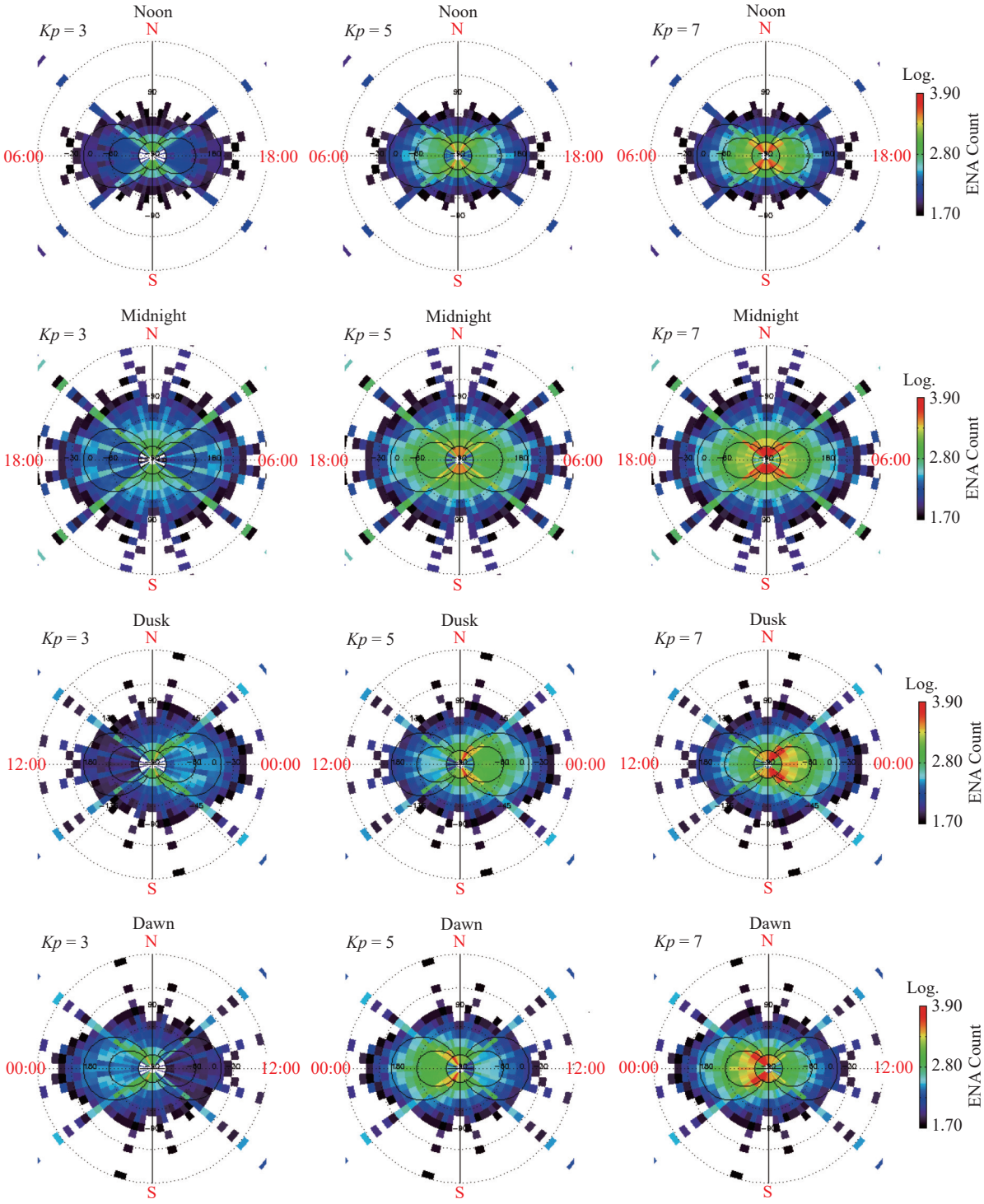


Fig. 3 Simulation ENA image with the integral time of 1 min for 4 feature positions under different geomagnetic activity conditions. The spatial angular resolution of each pixel is 6°×6°

In view of physics, the symmetry of south and north means that the energy ion input that causes the change of ion flux occurs in the closed magnetic field line region of low latitude, such as the magnetotail ion injection, the pitch angle diffusion of energy ions, *etc*. If there are direct inputs of solar wind ions at high latitude open magnetic field line region, it is possible to obtain the south-north asymmetric ENA images. Therefore,

Table 2 Maximum ENA counts

Kp index	3	5	7
Noon	1603.9397	3081.94775	5071.10938
Dusk	2944.28613	5501.90088	9027.37207
Night	1672.59656	3639.30688	6446.42285
Dawn	2944.28687	5501.91699	9027.36035

ENA imaging measurements in geosynchronous orbit are of innovative significance in magnetospheric physics.

The geostationary orbit satellite is equipped with both plasma detector and ENA imager, which makes the *in-situ* and remote data confirm each other[1,2,23]. ENA imaging inversion is global. The closer the satellite is to the ENA emission source, the stronger the ENA emission signal it receives and the smaller the relative error of ion flux inversion results at the corresponding satellite location, which is also an important area for in-situ measurements.

The time sequence of response of different payloads to geomagnetic activities also explains the causal sequence of particle events. The time scale of substorm events is about 30 min. A major geomagnetic storm can contain multiple continuous substorms. The high spatial and temporal resolution ENA measurement and inversion results[2] show that the azimuth of ion flux distribution evolves rapidly during the substorm, and the azimuth of the maximum ion flux region moves nearly 10 time zones in about 10 min. The source of particle input for such a rapidly moving of large energetic ion flux distribution remains a mystery. Tracing the source of the input that causes the change of ion flux is an important topic at present. Comparing the large and rapid evolution process of ion flux captured by *in-situ* measurements with the time sequence of global ENA imaging inversion results can help solve the above problems.

3 Conclusions

The above discussion indicates that ENA imaging measurements on geosynchronous orbit satellite have the innovative significance of expanding cognition in the field of space science. In a geostationary orbit, (1) the conjugated properties of ENA images indicate the north-south symmetry of precipitating ions, so as to investigate if injected ions coming from open/closed magnetic field regions; (2) energy particle *in-situ* measurements and ENA imaging are combined to investigate the causal sequence of energetic particle events in the ring current region. The above efforts aim to investigate the source and trigger mechanism of energy particles in geomagnetic active events and to upgrade the ENA imaging instruments and inversion model.

Geosynchronous orbit has a large family of satellites, which are very common in the application satellite sequence, such as meteorology, navigation, resource monitoring, *etc*., providing a lot of cooperating opportunities for the payload carrying. The design and development of a special ENA imager for the complex particle emission environment in geosynchronous orbit and the development of a 3D ENA imaging inversion model will become new hotspots in the field of magnetosphere physics.

References

[1] LU L, MCKENNA-LAWLOR S, CAO J B, *et al.* The causal sequence investigation of the ring current ion-flux increasing and the magnetotail ion injection during a major storm[J]. *Science China Earth Sciences*, 2016, **59**(1): 129-144

[2] LU L, MCKENNA-LAWLOR S, BALAZ J. Close up observation and inversion of low-altitude ENA emissions during a substorm event[J]. *Science China Earth Sciences*, 2019, **62**(6): 1024-1032

[3] MCKENNA-LAWLOR S, BALAZ J, STRHARSKY I, *et al.* The energetic NeUtral atom detector unit (NUADU) for China's double star mission and its calibration[J]. *Nuclear Instruments and Methods in Physics Research Section A: Accelerators, Spectrometers, Detectors and Associated Equipment*, 2004, **503**(3): 311-322

[4] LIU Z X, ESCOUBET C P, PU Z, *et al.* The double star mission[J]. *Annales Geophysicae*, 2005, **23**(8): 2707-2712

[5] BURCH J L. IMAGE mission overview[J]. *Space Science Reviews*, 2000, **91**(1): 1-14

[6] MCCOMAS D J, ALLEGRINI F, BALDONADO J, *et al.*

The two wide-angle imaging neutral-atom spectrometers (TWINS) NASA mission-of-opportunity[J]. *Space Science Reviews*, 2009, **142**(1): 157-231

[7] ROELOF E C. Energetic neutral atom image of a storm-time ring current[J]. *Geophysical Research Letters*, 1987, **14**(6): 652-655

[8] ROELOF E C, SKINNER A J. Extraction of ion distributions from magnetospheric ENA and EUV images[J]. *Space Science Reviews*, 2000, **91**(1/2): 437-459

[9] PEREZ J D, FOK M C, MOORE T E. Deconvolution of energetic neutral atom images of the Earth's magnetosphere[J]. *Space Science Reviews*, 2000, **91**(1/2): 421-436

[10] PEREZ J D, KOZLOWSKI G, C:SON-BRANDT P, *et al.* Initial ion equatorial pitch angle distributions from medium and high energy neutral atom images obtained by IMAGE[J]. *Geophysical Research Letters*, 2001, **28**(6): 1155-1158

[11] DEMAJISTRE R, ROELOF E C, BRANDT P C, *et al.* Retrieval of global magnetospheric ion distributions from high-energy neutral atom measurements made by the IMAGE/HENA instrument[J]. *Journal of Geophysical Research: Space Physics*, 2004, **109**(A4): A04214

[12] LU L, MCKENNA-LAWLOR S, BARABASH S, *et al.* Iterative inversion of global magnetospheric ion distributions using energetic neutral atom (ENA) images recorded by the NUADU/TC2 instrument[J]. *Annales Geophysicae*, 2008, **26**(6): 1641-1652

[13] LU L, YU Q L, LU Q. Near-approach imaging simulation of low-altitude ENA emissions by a LEO satellite[J]. *Frontiers in Astronomy and Space Sciences*, 2020, **7**: 35

[14] XING Z Y, ZHANG Q H, HAN D S, *et al.* Conjugate observations of the evolution of polar cap arcs in both hemispheres[J]. *Journal of Geophysical Research: Space Physics*, 2018, **123**(3): 1794-1805

[15] LU L, YANG C B, DONG Y J, *et al*. A deflection device for charged particles: CN, 104733069 A[P]. 2015-06-24 (路立, 杨垂柏, 董永进, 等. 一种带电粒子的偏转装置: 中国, 104733069 A[P]. 2015-06-24)

[16] SMITH P H, BEWTRA N K. Charge exchange lifetimes for ring current ions[J]. *Space Science Reviews*, 1978, **22**(3): 301-318

[17] RAIRDEN R L, FRANK L A, CRAVEN J D. Geocoronal imaging with dynamics explorer[J]. *Journal of Geophysical Research: Space Physics*, 1986, **91**(A12): 13613-13630

[18] TINSLEY B A, HODGES R R JR, ROHRBAUGH R P. Monte carlo models for the terrestrial exosphere over a solar cycle[J]. *Journal of Geophysical Research: Space Physics*, 1986, **91**(A12): 13631-13647

[19] BRANDT P C, BARABASH S, ROELOF E C, *et al.* Energetic neutral atom imaging at low altitudes from the Swedish microsatellite Astrid: Extraction of the equatorial ion distribution[J]. *Journal of Geophysical Research: Space Physics*, 2001, **106**(A11): 25731-25744

[20] GOLDSTEIN J, BISIKALO D V, SHEMATOVICH V I, *et al.* Analytical estimate for low-altitude ENA emissivity[J]. *Journal of Geophysical Research: Space Physics*, 2016, **121**(2): 1167-1191

[21] BRANDT P C, DEMAJISTRE R, ROELOF E C, *et al.* IMAGE/high-energy energetic neutral atom: Global energetic neutral atom imaging of the plasma sheet and ring current during substorms[J]. *Journal of Geophysical Research: Space Physics*, 2002, **107**(A12): 1454

[22] BRANDT P C, ROELOF E C, OHTANI S, *et al.* IMAGE/HENA: Pressure and current distributions during the 1 October 2002 storm[J]. *Advances in Space Research*, 2004, **33**(5): 719-722

[23] LU L, MCKENNA-LAWLOR S, BARABASH S, *et al.* Comparisons between ion distributions retrieved from ENA images of the ring current and contemporaneous, multipoint ion measurements recorded in situ during the major magnetic storm of 15 May 2005[J]. *Journal of Geophysical Research: Space Physics*, 2010, **115**(A12): A12218